

## WATER VAPOR IN NEARBY INFRARED GALAXIES AS PROBED BY *HERSCHEL*\*

CHENTAO YANG (杨辰涛)<sup>1,2,3</sup>, YU GAO (高煜)<sup>2</sup>, A. OMONT<sup>4,5</sup>, DAIZHONG LIU (刘岱钟)<sup>2,3</sup>, K. G. ISAAK<sup>6</sup>, D. DOWNES<sup>7</sup>, P. P. VAN DER WERF<sup>8</sup>, AND NANYAO LU<sup>9</sup>

Draft version July 9, 2018

### ABSTRACT

We report the first systematic study of the submillimeter water vapor rotational emission lines in infrared (IR) galaxies based on the Fourier Transform Spectrometer (FTS) data of *Herschel* SPIRE. Among the 176 galaxies with publicly available FTS data, 45 have at least one H<sub>2</sub>O emission line detected. The H<sub>2</sub>O line luminosities range from  $\sim 1 \times 10^5 L_{\odot}$  to  $\sim 5 \times 10^7 L_{\odot}$  while the total IR luminosities ( $L_{\text{IR}}$ ) have a similar spread ( $\sim 1 - 300 \times 10^{10} L_{\odot}$ ). In addition, emission lines of H<sub>2</sub>O<sup>+</sup> and H<sub>2</sub><sup>18</sup>O are also detected. H<sub>2</sub>O is found, for most galaxies, to be the strongest molecular emitter after CO in FTS spectra. The luminosity of the five most important H<sub>2</sub>O lines is near-linearly correlated with  $L_{\text{IR}}$ , no matter whether strong active galactic nucleus signature is present or not. However, the luminosity of H<sub>2</sub>O(2<sub>11</sub>–2<sub>02</sub>) and H<sub>2</sub>O(2<sub>20</sub>–2<sub>11</sub>) appears to increase slightly faster than linear with  $L_{\text{IR}}$ . Although the slope turns out to be slightly steeper when  $z \sim 2-4$  ULIRGs are included, the correlation is still closely linear. We find that  $L_{\text{H}_2\text{O}}/L_{\text{IR}}$  decreases with increasing  $f_{25}/f_{60}$ , but see no dependence on  $f_{60}/f_{100}$ , possibly indicating that very warm dust contributes little to the excitation of the submillimeter H<sub>2</sub>O lines. The average spectral line energy distribution (SLED) of the entire sample is consistent with individual SLEDs and the IR pumping plus collisional excitation model, showing that the strongest lines are H<sub>2</sub>O(2<sub>02</sub>–1<sub>11</sub>) and H<sub>2</sub>O(3<sub>21</sub>–3<sub>12</sub>).

*Keywords:* galaxies: ISM — galaxies: starburst — infrared: ISM — ISM: molecules  
(Online-only material: color figures)

### 1. INTRODUCTION

H<sub>2</sub>O can be one of the most abundant oxygen molecular carriers besides CO in the warm interstellar gas (but it is mostly locked in icy interstellar dust grains in cold regions of the Galaxy, e.g., Melnick & Bergin 2005; van Dishoeck et al. 2011). Nevertheless, the study of the rotational H<sub>2</sub>O line is always far more challenging than CO at low redshift. The main difficulty is from the contamination of the H<sub>2</sub>O in the Earth atmosphere. However, some pioneering research with the *Infrared Space Observatory* (covering  $\sim 2 - 200 \mu\text{m}$ ) (Kessler et al. 1996) of both star-forming regions within our Galaxy, like Orion (Harwit et al. 1998), and nearby galaxies, like Arp220 (González-Alfonso et al. 2004), NGC253 and NGC1068 (Goicoechea et al. 2005), and Mrk231 (González-Alfonso et al. 2008), revealed that H<sub>2</sub>O lines likely trace the local infrared radiation field (IRF) directly, thus provide a unique diagnostic probing the physical and chemical processes unlike other gas tracers like CO. The

*Herschel Space Observatory* (Pilbratt et al. 2010) with great improvement of sensitivity, angular resolution and band coverage offers an unprecedented opportunity to study the submillimeter regime of galaxies without atmospheric contamination, thus provides unique chances to observe the H<sub>2</sub>O lines within the SPIRE band (194–672  $\mu\text{m}$ , Griffin et al. 2010).

*Herschel* has revealed a wealth of submillimeter H<sub>2</sub>O lines in, e.g., Mrk231 (van der Werf et al. 2010; González-Alfonso et al. 2010, G-A10 hereafter), Arp220 (Rangwala et al. 2011; González-Alfonso et al. 2012, 2013), NGC4418 (González-Alfonso et al. 2012), NGC1068 (Spinoglio et al. 2012), NGC6240 (Meijerink et al. 2013) and M82 (Kamenetzky et al. 2012), from energy level  $E_{\text{up}}/k = 53$  K up to  $E_{\text{up}}/k = 642$  K. Moreover, some detections from ground in high- $z$  ultra-luminous IR galaxies (ULIRGs) were also reported (e.g. Omont et al. 2011; van der Werf et al. 2011; Combes et al. 2012; Omont et al. 2013; Riechers et al. 2013). H<sub>2</sub>O line strength is found to be comparable with neighboring high- $J$  CO lines ( $J = 8-7$  to  $J = 13-12$ ) in these studies.

By modeling the H<sub>2</sub>O excitation and dust continuum in Mrk231, G-A10 interpreted that collisional excitation from a cool extended region (610 pc, 41 K) is responsible for part of the low-lying line excitation, while IR pumping through far-IR photons by compact warm dense gas (120 pc, 95 K) excites high-lying lines and part of low-lying lines. The high abundance of H<sub>2</sub>O can be explained as a consequence of shocks/cosmic rays and X-ray dominated regions (XDR) chemistry (Meijerink et al. 2005), and/or an “undepleted chemistry” (G-A10). Therefore, H<sub>2</sub>O excitation is naturally linked to the local IRF, probing, e.g., the size and strength of the IR power source; tracing a different regime of gas than that of CO. Hence it is important to have a systematic study of the H<sub>2</sub>O lines in galaxies, for better understanding the gas excitation and physical processes within.

<sup>1</sup> Department of Astronomy, Beijing Normal University, Beijing 100875, China

<sup>2</sup> Purple Mountain Observatory/Key Lab of Radio Astronomy, Chinese Academy of Sciences, Nanjing 210008, China

<sup>3</sup> University of Chinese Academy of Sciences, Beijing, China

<sup>4</sup> Institut d’Astrophysique de Paris, UPMC Université Paris 06, UMR7095, F-75014, Paris, France

<sup>5</sup> CNRS, UMR7095, Institut d’Astrophysique de Paris, F-75014, Paris, France

<sup>6</sup> ESA Astrophysics Missions Division, ESTEC, PO Box 299, 2200 AG Noordwijk, The Netherlands

<sup>7</sup> Institut de Radioastronomie Millimétrique (IRAM), 300 rue de la Piscine, F-38406 Saint-Martin d’Hères, France

<sup>8</sup> Leiden Observatory, Leiden University, Post Office Box 9513, NL-2300 RA Leiden, The Netherlands

<sup>9</sup> Infrared Processing and Analysis Center, California Institute of Technology, MS 100-22, Pasadena, CA 91125, USA

\* *Herschel* is an ESA space observatory with science instruments provided by European-led Principal Investigator consortia and with important participation from NASA.

## 2. THE SAMPLE AND DATA REDUCTION

We used the *Herschel* Science Archive (HSA), containing both the SPIRE/Fourier Transform Spectrometer (FTS; Naylor et al. 2010) spectra at 450–1550GHz, and the PACS (Poglitsch et al. 2010) images at 70, 100 and 160  $\mu\text{m}$ . Our sample consists of 45 sources with at least one rotational  $\text{H}_2\text{O}$  transition detected among 176 nearby galaxies available. The data are from 10 projects including *HerCULES* (PI: P. van der Werf) with an  $\text{H}_2\text{O}$  detection rate  $\sim 80\%$  and *GOALS* (PI: N. Lu., a full list can be found here: <http://sfig.pmo.ac.cn/~yangcht/h2oSample.txt>). The typical SPIRE/FTS integration time is about several hours.

The data were reduced with HIPE v9 (Ott 2010). Basic steps of spectral data reduction contain background removal using off-axis detector subtraction and flux calibration with Neptune and Uranus, when available. Deglitch, flat field, calibration through HIPE, and brightness drift subtraction with *Scanamorphos* (Roussel 2012) have been used to reduce PACS images. All the  $\text{H}_2\text{O}$  emission line detections are above the  $3\sigma$  level. The instrumental sinc function has been adopted for the line fit using customized HIPE scripts, since the intrinsic line width is smaller than the instrumental resolution in most cases. However, the flux could be underestimated by  $\sim 20\%$  for few sources with very broad linewidth like Arp220, it is still insignificant when we consider the line fitting error ( $\sim 20\%$ ), the main source of the errors. Then we use the formula in Solomon et al. (1992) to convert line intensity ( $I_{\text{H}_2\text{O}}$ ) to  $L_{\text{H}_2\text{O}}$ , taking the luminosity distance  $D_L$  in Sanders et al. (2003) ( $H_0 = 75 \text{ km s}^{-1} \text{ Mpc}^{-1}$ ,  $\Omega_M = 0.3$ , and  $\Omega_\Lambda = 0.7$ ; Mould et al. 2000).

After convolving *Spitzer*/MIPS 24  $\mu\text{m}$ , PACS 70, 100, and 160  $\mu\text{m}$  images to match with the SPIRE beams (Swinyard et al. 2010) following Aniano et al. (2011), we determine whether the source is extended or not based on its radial profile as compared with that of the corresponding Gaussian point-spread functions (PSFs). We use the total IR luminosities (8–1000  $\mu\text{m}$ ) from Sanders et al. (2003) as the  $L_{\text{IR}}$  for point sources. For extended galaxies, in-beam  $L_{\text{IR}}$  is calculated to ensure that  $L_{\text{IR}}$  and  $L_{\text{H}_2\text{O}}$  are spatially matched. First, we take the weighting coefficients of Galametz et al. (2013) to combine MIPS 24, PACS 70, 100 and 160  $\mu\text{m}$  images into composite maps. Then the in-beam flux ratio between in-aperture and that of the entire source is derived with aperture photometries (FWHM of the Gaussian PSFs). It should be noticed that the practically measured area by SPIRE/FTS is not limited in the FWHM beam, we need an additional correction factor to account for this (D. Liu et al., in preparation). Applying this factor, we can then obtain the corrected in-beam fraction of the  $L_{\text{IR}}$  for extended sources.  $L_{\text{IR}}$  matched with the SPIRE beam can thus be obtained by applying this factor and the in-beam fraction to the global  $L_{\text{IR}}$  in Sanders et al. (2003). The full dataset containing  $L_{\text{IR}}$  and  $L_{\text{H}_2\text{O}}$  will be described in D. Liu et al. (in preparation). Since we take the global flux density ratios of 25–60  $\mu\text{m}$  ( $f_{25}/f_{60}$ ) and 60–100  $\mu\text{m}$  ( $f_{60}/f_{100}$ ) as the IR colors (flux densities from Sanders et al. 2003) in later analysis, we exclude the extended sources in these cases in order to keep the IR colors free from any contamination in spatial variations.

$\text{H}_2\text{O}$  lines are also detected in the mapping mode data of M82, NGC1068 and NGC253. However, we have dropped M82 mapping mode data because the very weak detection is only in the central detector and we already have a robust de-

tection in the single pointing mode. For NGC253, we add all the spectral data to obtain a global spectrum. For NGC1068, we have at least one  $\text{H}_2\text{O}$  line detection in seven detectors. These sources are obviously extended and excluded in the IR color analysis.

## 3. RESULTS AND DISCUSSION

In our sample we find that  $\text{H}_2\text{O}$  is the strongest molecular emitter after high- $J$  CO ( $J = 8-7$  to  $J = 13-12$ ) in the SPIRE band. In some cases ( $\sim 13\%$ ), e.g., ESO320-G030, the strength of  $\text{H}_2\text{O}(3_{21}-3_{12})$  is even stronger. Besides the  $\text{H}_2\text{O}$  emission lines,  $\text{H}_2\text{O}(1_{11}-0_{00})$  is detected in absorption in three sources, including Arp220 as reported by Rangwala et al. (2011).  $\text{H}_2\text{O}^+$  absorption lines were also detected in a few sources (D. Liu et al. in preparation). In addition, emission lines of  $\text{H}_2\text{O}^+$  and  $\text{H}_2^{18}\text{O}$  are detected (Section 3.3). Those ionic molecules are the intermediate species for the main route of gas-phase  $\text{H}_2\text{O}$  formation.

### 3.1. Relation between $\text{H}_2\text{O}$ and IR Luminosities

The correlation between  $L_{\text{H}_2\text{O}}$  for different transitions and  $L_{\text{IR}}$  was analyzed by two different methods: a Bayesian approach, LINMIX\_ERR (Kelly 2007), and the nonLinear  $\chi^2$  fitting routine, MPFIT (Markwardt 2009). In Figure 1 we plot the luminosities of  $\text{H}_2\text{O}(1_{11}-0_{00})$ ,  $\text{H}_2\text{O}(2_{02}-1_{11})$ ,  $\text{H}_2\text{O}(2_{11}-2_{02})$ ,  $\text{H}_2\text{O}(2_{20}-2_{11})$ ,  $\text{H}_2\text{O}(3_{12}-3_{03})$ ,  $\text{H}_2\text{O}(3_{21}-3_{12})$ ,  $\text{H}_2\text{O}(4_{22}-4_{13})$  and  $\text{H}_2\text{O}(5_{23}-5_{14})$  (lines 1 to 8 hereafter) against the corresponding  $L_{\text{IR}}$ . In addition to our sample, we also include five high- $z$  ULIRGs (Omont et al. 2013, see online Table 4) and HLSJ0918+5144 (Combes et al. 2012) in our fit for line 2 and 3 (Figure 1). The QSO APM08279+5255 at  $z = 3.9$  (van der Werf et al. 2011) is also added for comparison.

The two fitting methods yield similar results in log–log space over four orders of magnitude of the luminosity range. The fit can be described as

$$\log L_{\text{H}_2\text{O}} = \alpha \log L_{\text{IR}} + \beta. \quad (1)$$

The derived parameters are listed in Table 1. All values of  $\alpha$  are close to 1, i.e., a linear relation, though the  $\alpha$  given by the Bayesian approach are closer to linear. However, the  $\alpha$  of lines 3 and 4 are a bit higher than that of other lines. This is weakly significant when we consider the errors. The  $\alpha$  of lines 2 and 3 are consistent with Omont et al. (2013). As the slopes are close to linear, we perform an additional linear fit by fixing  $\alpha = 1$ , and use  $\chi^2$  fitting to determine the constant ratios between  $L_{\text{H}_2\text{O}}$  and  $L_{\text{IR}}$ . These ratios vary from  $3.3 \times 10^{-6}$  for  $\text{H}_2\text{O}(1_{11}-0_{00})$  to  $1.1 \times 10^{-5}$  for  $\text{H}_2\text{O}(3_{21}-3_{12})$  (see the gray dashed lines and text in Figure 1 and Table 1). Because the detections of lines 1, 7 and 8 are not statistically significant, more data are needed to solidify the fits. In Figure 1, we find most of the  $\text{H}_2\text{O}(2_{11}-2_{02})$  and  $\text{H}_2\text{O}(3_{21}-3_{12})$  upper limits for the non-detections are consistent with the correlation. All the (U)LIRGs have a strong  $\text{H}_2\text{O}$  emission compatible with the correlation pointing out to a rather large  $\text{H}_2\text{O}$  abundance as known in shocked regions (e.g. G-A10; Harwit et al. 1998). Unlike the case in the Orion Bar, the proto-typical photo-dissociation region (PDR), where CO lines are a factor  $\gtrsim 50$  stronger than the  $\text{H}_2\text{O}$  lines, the high  $\text{H}_2\text{O}/\text{CO}$  ratio of most sources in our sample makes it unlikely that those strong  $\text{H}_2\text{O}$  emission originate in classical PDRs (e.g., G-A10). The high CO/ $\text{H}_2\text{O}$  ratio in M82 ( $\sim 40$ ; Weiß et al. 2010) indicates that it is dominated by classical PDRs, and thus has much

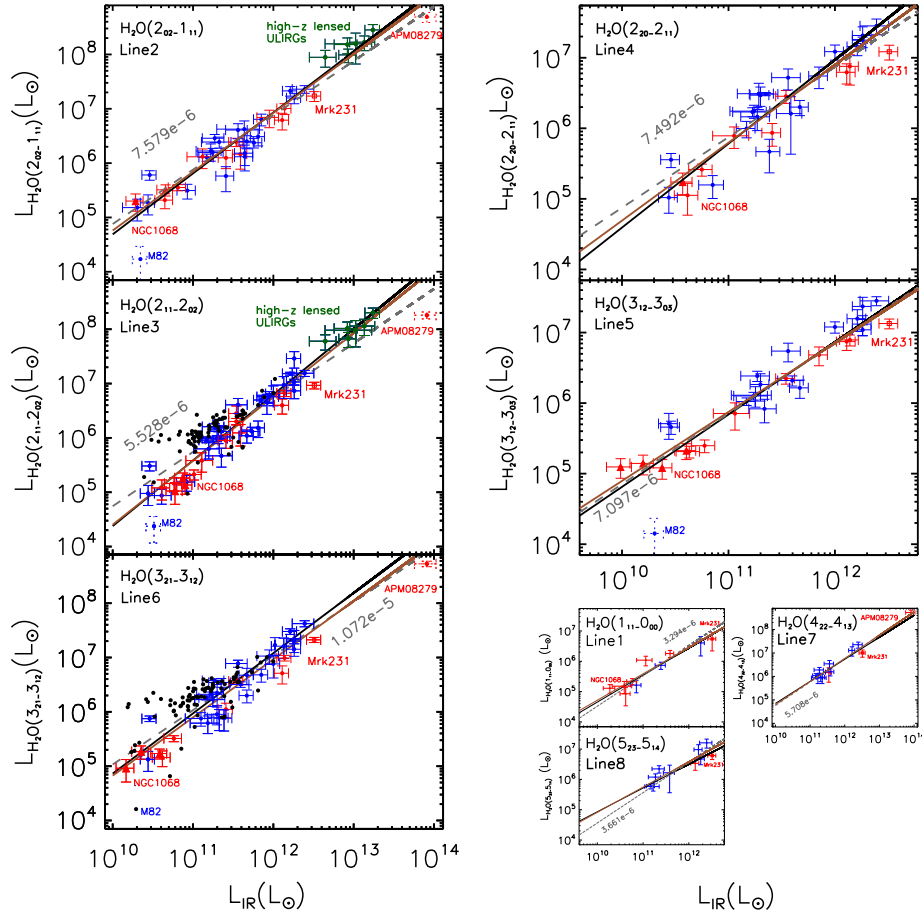


**Figure 1.** Correlation between  $L_{\text{H}_2\text{O}}$  and the corresponding  $L_{\text{IR}}$  of our sample. Fitted lines by MPFIT and LINMIX\_ERR are shown in black and brown lines, respectively, while gray lines are the linear fitting with fixed slope ( $\alpha = 1$ ). Red, blue, green and black dots represent strong-AGN, HII+mild-AGN-dominated galaxies, high- $z$  ULIRGs, and upper limits for non-detections, respectively. Solid triangles are the mapping mode data of NGC1068. Mrk231 is marked in red squares. M82 and APM08279+5255, marked with dashed error bars, are excluded from the fitting. (A color version of this figure is available in the online journal.)

**Table 1**  
Fitted Parameters of the Correlations between  $\text{H}_2\text{O}$  Lines and  $L_{\text{IR}}$  (Equation (1))

$\text{H}_2\text{O}$ Line	$\nu_{\text{rest}}$ (GHz)	$\alpha_{\chi^2}$	$\alpha_{\text{Bayes}}$	$\beta_{\chi^2}$	$\beta_{\text{Bayes}}$	$\langle L_{\text{H}_2\text{O}}/L_{\text{IR}} \rangle$
1, $1_{11}-0_{00}^a$	1113.343	$0.89 \pm 0.09$	$0.86 \pm 0.17$	$-4.24 \pm 1.06$	$-3.76 \pm 1.94$	$3.29 \times 10^{-6}$
2, $2_{02}-1_{11}$	987.927	$1.12 \pm 0.04$	$1.08 \pm 0.05$	$-6.52 \pm 0.47$	$-6.07 \pm 0.59$	$7.58 \times 10^{-6}$
3, $2_{11}-2_{02}$	752.033	$1.21 \pm 0.04$	$1.18 \pm 0.06$	$-7.72 \pm 0.49$	$-7.34 \pm 0.67$	$5.53 \times 10^{-6}$
4, $2_{20}-2_{11}$	1228.789	$1.19 \pm 0.06$	$1.10 \pm 0.08$	$-7.30 \pm 0.69$	$-6.33 \pm 0.97$	$7.49 \times 10^{-6}$
5, $3_{12}-3_{03}$	1097.365	$1.03 \pm 0.04$	$0.98 \pm 0.06$	$-5.45 \pm 0.51$	$-4.88 \pm 0.65$	$7.10 \times 10^{-6}$
6, $3_{21}-3_{12}$	1162.912	$1.11 \pm 0.05$	$1.07 \pm 0.09$	$-6.22 \pm 0.57$	$-5.88 \pm 1.05$	$1.07 \times 10^{-5}$
7, $4_{22}-4_{13}^a$	1207.639	$0.94 \pm 0.12$	$0.84 \pm 0.22$	$-2.91 \pm 1.12$	$-3.43 \pm 2.51$	$5.71 \times 10^{-6}$
8, $5_{23}-5_{12}^a$	1410.618	$0.78 \pm 0.10$	$0.99 \pm 0.19$	$-4.56 \pm 1.37$	$-4.93 \pm 2.30$	$3.66 \times 10^{-6}$

**Notes.** <sup>a</sup>: The resulting parameters of  $1_{11}-0_{00}$ ,  $4_{22}-4_{13}$  and  $5_{23}-5_{12}$  contain large uncertainties due to the small sample size.  $\alpha_{\chi^2}$  and  $\beta_{\chi^2}$  are the slope and intercept from  $\chi^2$  fitting, while  $\alpha_{\text{Bayes}}$  and  $\beta_{\text{Bayes}}$  are from the Bayesian method.

weaker  $\text{H}_2\text{O}$  lines. As in Weiß et al. (2010), the  $\text{H}_2\text{O}$  lines in M82 are found to be very weak, nearly an order of magnitude below the correlation. It would be important to analyze the weak  $\text{H}_2\text{O}$  emission in other galaxies like M82, but it is outside the scope of this work. Therefore, we excluded M82 from our fit. Additionally, when we fit the correlations for  $L_{\text{H}_2\text{O}-2}$  and  $L_{\text{H}_2\text{O}-3}$  without high- $z$  ULIRGs, we get slightly lower slopes. This means that high- $z$  ULIRGs at the high  $L_{\text{IR}}$  end have slightly higher  $L_{\text{H}_2\text{O}}/L_{\text{IR}}$ .

The linear correlation could be the result of the very intense far-IR radiation via IR pumping. After the absorption of far-IR photons, the upper level  $\text{H}_2\text{O}$  molecules cascade toward the lines we observed in an approximately constant fraction. Thus the  $\text{H}_2\text{O}$  luminosity should be linearly correlated with the IR emission. Though detailed excitation modeling is needed, this linear correlation already shows the importance of IR pumping.

Using the NASA/IPAC Extragalactic Database (NED), we

**Table 2**  
Correlations between  $(L_{\text{H}_2\text{O}}/L_{\text{IR}})/L_{\text{IR}}$ , Different  $\text{H}_2\text{O}$  Line Ratios and IR Colors,  $L_{\text{IR}}$ .

Ratio	$R_{\log(f_{25}/f_{60})}$	$R_{\log(f_{60}/f_{100})}$	$R_{\log(L_{\text{IR}})}$	$\langle \text{strong-AGN} \rangle$	$\langle \text{HII+mild-AGN} \rangle$
2/IR, $2_{02}-1_{11}$ /IR	-0.51	-0.25	-0.10	$6.4 \times 10^{-6}$	$9.2 \times 10^{-6}$
3/IR, $2_{11}-2_{02}$ /IR	-0.51	0.17	-0.39	$3.8 \times 10^{-6}$	$5.8 \times 10^{-6}$
4/IR, $2_{20}-2_{11}$ /IR	-0.55	-0.03	-0.21	$5.0 \times 10^{-6}$	$9.2 \times 10^{-6}$
5/IR, $3_{12}-3_{03}$ /IR	-0.40	-0.02	-0.18	$5.1 \times 10^{-6}$	$9.4 \times 10^{-6}$
6/IR, $3_{21}-3_{12}$ /IR	-0.67	-0.07	-0.17	$6.7 \times 10^{-6}$	$10.8 \times 10^{-6}$
2/3, $2_{02}-1_{11}/2_{11}-1_{02}$	0.16	-0.50	-0.38	1.50	1.52
2/4, $2_{02}-1_{11}/2_{20}-2_{11}$	0.16	-0.38	-0.47	1.09	1.09
2/5, $2_{02}-1_{11}/3_{12}-3_{03}$	-0.11	-0.28	0.25	1.14	0.88
2/6, $2_{02}-1_{11}/3_{21}-3_{12}$	0.56	-0.07	-0.20	0.87	0.72
3/4, $2_{11}-2_{02}/2_{20}-2_{11}$	0.10	0.35	0.08	0.61	0.63
3/5, $2_{11}-2_{02}/3_{12}-3_{03}$	-0.26	0.14	0.47	0.62	0.52
3/6, $2_{11}-2_{02}/3_{21}-3_{12}$	0.47	0.11	0.15	0.50	0.48
4/5, $2_{20}-2_{11}/3_{12}-3_{03}$	-0.15	-0.11	0.38	1.00	0.58
4/6, $2_{20}-2_{11}/3_{21}-3_{12}$	0.37	0.09	0.19	0.73	0.62
5/6, $3_{12}-3_{03}/3_{21}-3_{12}$	0.53	0.17	-0.21	0.69	0.65

**Notes.**  $R_{\log(f_{25}/f_{60})}$ ,  $R_{\log(f_{60}/f_{100})}$  and  $R_{\log(L_{\text{IR}})}$  are the correlation coefficients between  $\log[(L_{\text{H}_2\text{O}}/L_{\text{IR}})/L_{\text{IR}}]$ ,  $\log[(L_{\text{H}_2\text{O}}/L_{\text{IR}})_a/(L_{\text{H}_2\text{O}}/L_{\text{IR}})_b]$  and  $\log(f_{25}/f_{60})$ ,  $\log(f_{60}/f_{100})$ ,  $\log(L_{\text{IR}})$  respectively (see text).  $\langle \text{strong-AGN} \rangle$  and  $\langle \text{HII+mild-AGN} \rangle$  are the error weighted mean values of  $(L_{\text{H}_2\text{O}}/L_{\text{IR}})/L_{\text{IR}}$  and  $(L_{\text{H}_2\text{O}}/L_{\text{IR}})_a/(L_{\text{H}_2\text{O}}/L_{\text{IR}})_b$  for strong-AGN and star-forming dominated galaxies (see text), respectively.

have separated our sample into two groups: optically identified strong-active galactic nucleus (AGN) dominated (Seyfert types 1 and 2) and star-forming-dominated galaxies possibly with mild AGNs (classes HII, composite and LINER of Kewley et al. (2006), hereafter "HII+mild-AGN"), as red and blue points in Figure 1, respectively. There is no obvious difference between these two groups and they both exhibit similar correlations. This implies that both strong-AGN and HII+mild-AGN sources behave similarly in  $\text{H}_2\text{O}$  emission, and a strong AGN may have little impact on the  $\text{H}_2\text{O}$  excitation. Although the number of statistics is small, the detection rate of HII+mild-AGN ( $\sim 3.2\%$ ) is lower than strong AGN ( $\sim 12.4\%$ ) for  $\text{H}_2\text{O}(1_{11}-0_{00})$ . The remaining  $\text{H}_2\text{O}$  lines have comparable detection rates of both kinds, and line 2 and 3 have the highest detection rate of about 30%. The absence of and apparent significant AGN contribution indicates that an AGN may not be the main power source of the  $\text{H}_2\text{O}$  excitation. The origin of such abundant  $\text{H}_2\text{O}$  reservoir might thus favor an undepleted chemistry or shocks/cosmic rays rather than XDR chemistry (G-A10).

We then analyzed the correlation between  $L_{\text{H}_2\text{O}}/L_{\text{IR}}$  and the IR colors, along with the  $L_{\text{IR}}$  (Figure 2 and Table 2). We dismiss lines 1, 7 and 8 here for their insignificant statistics. Hardly has any correlation been found between  $L_{\text{H}_2\text{O}}/L_{\text{IR}}$  and  $f_{60}/f_{100}$  (Table 2). We find, however, that  $L_{\text{H}_2\text{O}}/L_{\text{IR}}$  ratios decrease with the increasing  $f_{25}/f_{60}$ , with significant correlation coefficients ( $R \sim -0.5$ ). A similar correlation has also been found in lines 7 and 8 though with low statistics. This correlation may be explained by a smaller contribution to the submillimeter  $\text{H}_2\text{O}$  line excitation from very warm dust radiation (dust temperature  $T_d \sim 110\text{K}$ ) than from warm dust ( $T_d \sim 50\text{K}$ ). We also find that line 6 has the largest  $R \sim -0.7$ , possibly indicating that this transition is more sensitive to  $T_d$  than others. There is no significant correlation between  $L_{\text{H}_2\text{O}}/L_{\text{IR}}$  and  $L_{\text{IR}}$  except for line 3 ( $R \sim 0.4$ ) as shown in the second column of Figure 2 and in Table 2. This seems to be consistent with the slightly super-linear relation found for  $L_{\text{H}_2\text{O}-3}$  with  $L_{\text{IR}}$  (Figure 1). The non-variation of  $L_{\text{H}_2\text{O}}/L_{\text{IR}}$  with  $L_{\text{IR}}$  for most lines confirms the validity of the near-linear

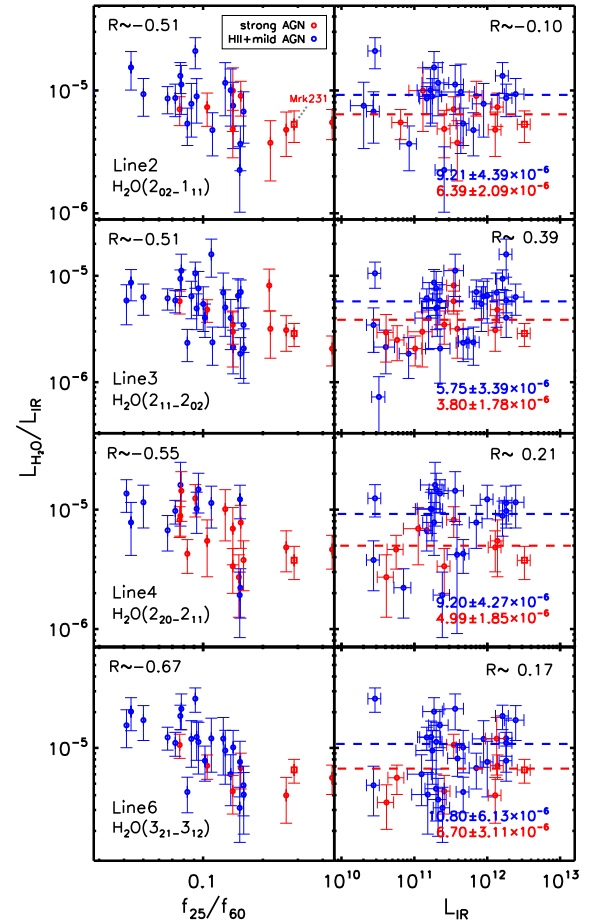


**Figure 2.**  $L_{\text{H}_2\text{O}}/L_{\text{IR}}$  versus  $f_{25}/f_{60}$  and  $L_{\text{IR}}$ , respectively. From top to bottom, each row displays the values of lines 2,3,4 & 6 as examples. Averaged values of  $L_{\text{H}_2\text{O}}/L_{\text{IR}}$  of strong-AGN and HII+mild-AGN-dominated sources are shown in red and blue text and dashed lines in the second column.  $R$  in each panel is the correlation coefficient. Mrk231 is shown in red squares. Blue and red colors are the same as in Figure 1.

relations in Figure 1.

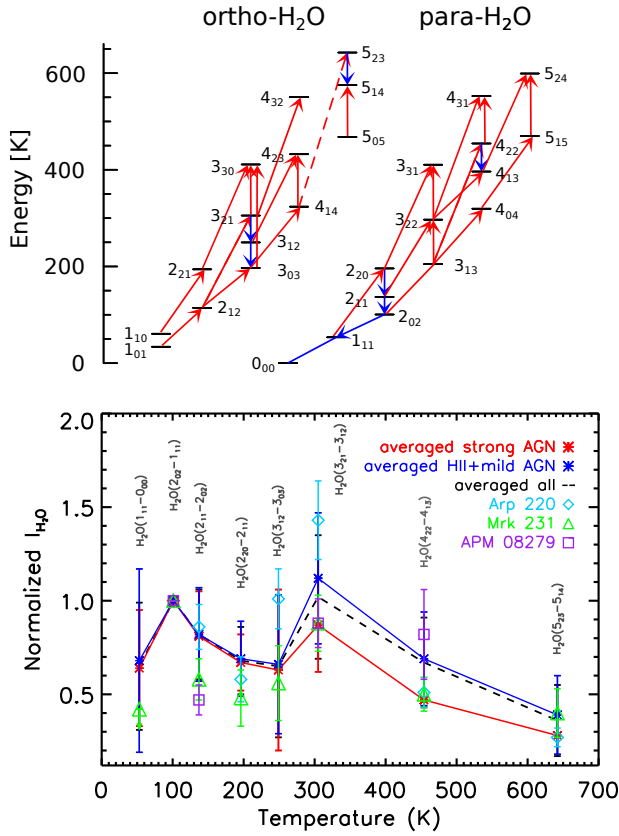


**Figure 3.** Upper panel shows the H<sub>2</sub>O energy level diagram. Among the red lines that indicate the main possible IR pumping paths, the solid lines show the observed absorption lines in Mrk231, Arp220 and NGC4418 (G-A10; González-Alfonso et al. 2012). Blue lines are the transitions we detected. The lower panel shows the  $I_{\text{H}_2\text{O}(2_{02}-1_{11})}$  normalized H<sub>2</sub>O intensities (in Jy km s<sup>-1</sup>). The black dashed line represents the average values of the whole sample, while red and blue points and lines are those of the strong-AGN and HII+mild-AGN-dominated galaxies, respectively. Green and light blue symbols represent Mrk231 (G-A10) and Arp220 (Rangwala et al. 2011), respectively. Purple squares represent the lensed QSO APM08279+5255 (van der Werf et al. 2011). (A color version of this figure is available in the online journal.)

Again, we here separate the sources into strong-AGN and HII+mild-AGN as in Figure 1. It appears that strong AGNs, on average, have higher  $f_{25}/f_{60}$  compared with the others. This is a well-known property of AGN sources that have more very warm dust than starburst sources (e.g., Younger et al. 2009). However, both strong-AGN and HII+mild-AGN species show a similar trend for the variation of  $L_{\text{H}_2\text{O}}/L_{\text{IR}}$  with  $f_{25}/f_{60}$ . Their different IR colors might cause the average value of  $L_{\text{H}_2\text{O}}/L_{\text{IR}}$  in strong AGNs to be slightly lower, about 40%, than in HII+mild-AGN sources for all lines (Figure 2 and Table 2), but the difference is hardly significant.

### 3.2. H<sub>2</sub>O Line Ratios and the Average Spectral Line Energy Distribution (SLED)

Line ratios between different transitions could help us understand the excitation of H<sub>2</sub>O and the physical condition of the warm dense gas. Thus we compare the H<sub>2</sub>O line ratios with IR colors and luminosities. As discussed in Section 2, different transitions have various beam sizes. In order to compare different H<sub>2</sub>O transitions, we have to remove this beam size dependence. We simply do this by dividing  $L_{\text{H}_2\text{O}}$  by  $L_{\text{IR}}$  since they are linearly correlated. Thus

$(L_{\text{H}_2\text{O}}/L_{\text{IR}})_a/(L_{\text{H}_2\text{O}}/L_{\text{IR}})_b$  ( $a/b^{11}$  hereafter) could represent the true luminosity ratio between two H<sub>2</sub>O lines, a and b. Table 2 lists the results. In Figure 2,  $(L_{\text{H}_2\text{O}}/L_{\text{IR}})_6$  has the steepest dependence on  $f_{25}/f_{60}$  compared with other lines. Thus the ratio between  $L_{\text{H}_2\text{O}}/L_{\text{IR}}$  of any other line and  $(L_{\text{H}_2\text{O}}/L_{\text{IR}})_6$  should have a correlation with  $f_{25}/f_{60}$ . Indeed, as we can see in the table, where the  $R$  for line ratios 2/6, 3/6 and 5/6 versus  $f_{25}/f_{60}$  is  $\gtrsim 0.5$ . Also the line ratio 2/3 decreases with increasing  $f_{60}/f_{100}$  ( $R \sim -0.5$ ). Although there are some  $R$  close to  $\pm 0.5$  for the correlation between  $I_{\text{H}_2\text{O}}/L_{\text{IR}}$  and  $L_{\text{IR}}$ , these trends may not be real for they are within the error. The low line ratio 2/6 in Table 2 might indicate that IR pumping is important since collisional excitation alone can not explain the high intensities of the high-lying lines compared with low-lying lines (e.g., G-A10).

In order to have a general view of the H<sub>2</sub>O excitation, we calculate the error-weighted average line intensity ratios with respect to H<sub>2</sub>O(2<sub>02</sub>–1<sub>11</sub>). In Figure 3, the upper panel shows the H<sub>2</sub>O energy level diagram. The lower panel of Figure 3 shows an average H<sub>2</sub>O SLED together with SLEDs taken from previous case studies (G-A10; van der Werf et al. 2011; Rangwala et al. 2011). The individual studies agree well with our averaged SLED. All SLEDs show two peaks at H<sub>2</sub>O(2<sub>02</sub>–1<sub>11</sub>) and H<sub>2</sub>O(3<sub>21</sub>–3<sub>12</sub>), and the latter is slightly stronger. The explanation for the strong high-lying peak could be that the IR spectral energy distribution (SED) peaks are close to 75  $\mu\text{m}$  which could result in higher IR pumping efficiency considering the possibility of IR pumping at 75  $\mu\text{m}$  (Figure 3, upper panel) which is the main power source of H<sub>2</sub>O(3<sub>21</sub>–3<sub>12</sub>) and H<sub>2</sub>O(3<sub>12</sub>–3<sub>03</sub>) (G-A10). However, we should be cautious in this interpretation because the H<sub>2</sub>O line intensities depend not only on the excitation conditions, but also on the intrinsic line strengths of the H<sub>2</sub>O molecule. Detailed excitation modeling is therefore needed. The high-lying lines to H<sub>2</sub>O(2<sub>02</sub>–1<sub>11</sub>) ratios in HII+mild-AGNs appear a bit stronger than strong-AGNs (Figure 3 and Table 2). In Section 3.1, we find that the high-lying lines have steeper anticorrelation on  $f_{25}/f_{60}$ , thus strong AGNs, with higher  $f_{25}/f_{60}$ , are expected to show lower high-lying lines to H<sub>2</sub>O(2<sub>02</sub>–1<sub>11</sub>) ratios.

### 3.3. Emission Lines of H<sub>2</sub>O-related Ionic and Isotope Molecules

Besides H<sub>2</sub>O, the related ionic and <sup>18</sup>O isotope molecular emission lines are also found. H<sub>2</sub>O<sup>+</sup> forms via ionization of H and H<sub>2</sub>, after the combination of H<sub>2</sub>, it forms H<sub>3</sub>O<sup>+</sup>, and the recombination with electrons leads to OH and H<sub>2</sub>O (Hollenbach et al. 2012). Among 45 H<sub>2</sub>O-detected sources, 5 of them have H<sub>2</sub>O<sup>+</sup>(1<sub>11</sub>–0<sub>00</sub>, J<sub>3/2,1/2</sub>) (1115.204 GHz), another 5 have H<sub>2</sub>O<sup>+</sup>(1<sub>11</sub>–0<sub>00</sub>, J<sub>1/2,1/2</sub>) (1139.561 GHz), 12 of them have H<sub>2</sub>O<sup>+</sup>(2<sub>02</sub>–1<sub>11</sub>, J<sub>3/2,3/2</sub>) (746.194 GHz), 7 sources have H<sub>2</sub>O<sup>+</sup>(2<sub>02</sub>–1<sub>11</sub>, J<sub>5/2,3/2</sub>) (742.033 GHz) and 3 have H<sub>2</sub><sup>18</sup>O(3<sub>21</sub>–3<sub>12</sub>) (1136.704 GHz) detected. Both strong-AGN- and HII+mild-AGN-dominated galaxies are among these detections. We find their luminosities to be tightly correlated with those of the related H<sub>2</sub>O transitions. Taking H<sub>2</sub>O<sup>+</sup>(2<sub>02</sub>–1<sub>11</sub>, J<sub>3/2,3/2</sub>) that has the largest number of detections for an example, the luminosities of H<sub>2</sub>O<sup>+</sup>(2<sub>02</sub>–1<sub>11</sub>, J<sub>3/2,3/2</sub>) and H<sub>2</sub>O(2<sub>02</sub>–1<sub>11</sub>) perfectly fit a linear correlation. H<sub>2</sub>O<sup>+</sup>(2<sub>02</sub>–1<sub>11</sub>) lines are about 4.5 times weaker than H<sub>2</sub>O(2<sub>02</sub>–1<sub>11</sub>), and

<sup>11</sup> a, b represent different H<sub>2</sub>O lines at different frequencies with different FTS beamsizes.

2.5 times weaker than  $\text{H}_2\text{O}(2_{11}-2_{02})$ , while the strength of  $\text{H}_2\text{O}^+(1_{11}-0_{00})$  is almost the same as that of  $\text{H}_2\text{O}(1_{11}-0_{00})$ . These preliminary results are important for further observations of those ionic diagnostic lines in high- $z$  galaxies, although the number of the sources ( $\lesssim 10$ ) is not sufficient to draw any concrete conclusion at this stage.

#### 4. CONCLUSIONS

$\text{H}_2\text{O}$  is found to be the second strongest molecular emitter in our sample of 45 nearby IR galaxies after high- $J$  CO lines within the SPIRE/FTS band. Near-linear correlations have been found between various  $\text{H}_2\text{O}$  rotational transitions and corresponding  $L_{\text{IR}}$ , whereas  $\text{H}_2\text{O}(2_{11}-2_{02})$  and  $\text{H}_2\text{O}(2_{20}-2_{11})$  may have slightly steeper slopes. The ratios of  $L_{\text{H}_2\text{O}}/L_{\text{IR}}$  vary with  $f_{25}/f_{60}$ , while nearly no any trend with  $f_{60}/f_{100}$  and  $L_{\text{IR}}$  has been found, indicating that very warm dust contributes little to the  $\text{H}_2\text{O}$  excitation. The near constant  $L_{\text{H}_2\text{O}}/L_{\text{IR}}$  ratios reveal an intrinsic linear correlation, no matter whether a strong AGN is present or not. We find no significant difference in the correlation between strong-AGN and star-forming-dominated galaxies, although strong AGNs might have slightly smaller average ratios  $L_{\text{H}_2\text{O}}/L_{\text{IR}}$ . And in less than one third of both kinds of galaxies, related ionic  $\text{H}_2\text{O}^+$  emission lines have been detected, while their strength tightly correlates with that of the corresponding  $\text{H}_2\text{O}$  lines.  $\text{H}_2^{18}\text{O}$  isotope line emission is also detected in three sources. It seems that the IR pumping at  $75\mu\text{m}$ , the IR SED peak, is most important in excitation of high-lying  $\text{H}_2\text{O}$  lines in these IR galaxies. Nevertheless, detailed modeling is needed, e.g. large velocity gradient or XDR models, in order to derive some physical parameters of the  $\text{H}_2\text{O}$  excitation and to provide a quantitative diagnostic tool of the IR radiation field and warm dense gas in galaxies other than CO lines.

This research is based on the data from HSA and is partially supported by the NSF of China (No. 11173059).

*Facility: Herschel*

#### REFERENCES

- Aniano, G., Draine, B. T., Gordon, K. D., & Sandstorm, K., 2011, *PASP*, 123, 1218
- Combes, F., Rex, M., Rawle, T. D., et al. 2012, *A&A*, 538, L4
- Galametz, M., Kennicutt, R. C., Calzetti, D., et al. 2013, *MNRAS*, 431, 1956
- Goicoechea, J. R., Martín-Pintado, J., Cernicharo, J., 2005, *ApJ*, 619, 291
- González-Alfonso, E., Smith, H. A., Fischer, J., Cernicharo, J., 2004, *ApJ*, 613, 247
- González-Alfonso, E., Smith, H. A., Ashby, M. L. N., et al. 2008, *ApJ*, 675, 303
- González-Alfonso, E., et al. 2010 *A&A* 518, L43
- González-Alfonso, E., Fischer, J., Graciá-Carpio, J., et al. 2012, *A&A*, 541, A4
- González-Alfonso, E., Fischer, J., Bruderer, S., et al. 2013, *A&A*, 550, A25
- Griffin, M. J., Abergel, A., Abreu, A., et al. 2010, *A&A*, 518, L3
- Harwit, M., Neufeld, D. A., Melnick, G. J. & Kaufman, M. J. 1998, *ApJ*, 497, L105
- Hollenbach, D., Kaufman, M. J., Neufeld, D., et al. 2012, *ApJ*, 754, 105
- Kamenetzky, J., Glenn, J., Rangwala, N., et al. 2012, *ApJ*, 753, 70
- Kessler, M. F., Steinz, J. A., Anderegg, M. E., et al. 1996, *A&A*, 315, L27
- Kelly, B. C., 2007, *ApJ*, 665, 1489
- Kewley, L. J., Groves, B., Kauffmann, G., Heckman, T. 2006, *MNRAS*, 372, 961
- Markwardt, C. B., 2009, *ASPC*, 411, 251
- Meijerink, R., Spaans, M., 2005, *A&A*, 436, 397
- Meijerink, R., Kristensen, L. E., et al. 2013, *ApJ*, 762, L16
- Melnick, G. J. and Bergin, E. A., 2005, *Advances in Space Research*, 36, 1027
- Mould, J. R., Huchra, J. P., Freedman, W. L., et al. 2000, *ApJ*, 529, 786
- Naylor, D. A., Baluteau, J.-P. et al. 2010, in *Society of Photo-Optical Instrumentation Engineers (SPIE) Conference Series*, Vol. 7731, Society of Photo-Optical Instrumentation Engineers (SPIE) Conference Series
- Omont, A., Neri, R., Cox, P., et al. 2011, *A&A*, 530, L3
- Omont, A., Yang, C., Cox, P., et al. 2013, *A&A*, 551, A115
- Ott, S. 2010, *ASP Conference Series*, 434, 139
- Pilbratt, G.L., Riedinger, J.R., Passvogel, T. et al. 2010, *A&A*, 518, L1
- Poglitsch, A., Waelkens, C., Geis, N. et al. 2010, *A&A*, 518, L2
- Rangwala, N., Maloney, P. R., Glenn, J., et al. 2011, *ApJ*, 743, 94
- Riechers, D. A. Bradford, C. M., et al. 2013, *Nature*, 496, 329
- Roussel, H., 2012, arXiv:1205.2576
- Sanders, D. B., Mazzarella, J. M., et al. 2003, *AJ*, 126, 1067
- Solomon, P.M., Downes, D., & Radford, S., 1992, *ApJ*, 398, L29
- Spinoglio, L., Pereira-Santaella, M., et al. 2012 *ApJ*, 758, 108
- Swinyard, B. M., Ade, P., Baluteau, J.-P., et al. 2010, *A&A*, 518, L4
- van der Werf, P. P., Berciano Alba, A., Spaans, M., et al. 2011, *ApJ*, 741, L38
- van der Werf, P. P., Isaak, K. G., Meijerink, R., et al. 2010, *A&A*, 518, L42
- van Dishoeck, E. F., Kristensen, L. E., Benz, A. O., et al. 2011, *PASP*, 123, 138
- Weiß, A., Requena-Torres, M. A., Güsten, R., 2010, *A&A*, 521, L1
- Younger, J. D., Hayward, C. C., Narayanan, D., et al. 2009, *MNRAS*, 396, L66